AGU PUBLICATIONS

Geophysical Research Letters

RESEARCH LETTER
10.1002/2017GL075763

Key Points:
- Substorm onset location is related to the morphology of the nightside ionospheric convection pattern
- Substorm local time-related asymmetries override those associated with IMF B_y
- Substorm onset local time is associated with an enhancement, reduction or mirroring of the expected B_y asymmetry

Correspondence to:
A. Grocott,
a.grocott@lancaster.ac.uk

Citation:
Grocott, A., Laurens, H. J., & Wild, J. A. (2017). Nightside ionospheric convection asymmetries during the early substorm expansion phase: Relationship to onset local time. *Geophysical Research Letters*, *44*. https://doi.org/10.1002/2017GL075763

Received 20 SEP 2017
Accepted 11 NOV 2017
Accepted article online 15 NOV 2017

Nightside Ionospheric Convection Asymmetries During the Early Substorm Expansion Phase: Relationship to Onset Local Time

A. Grocott[1], **H. J. Laurens**[1], **and J. A. Wild**[1]

[1] Physics Department, Lancaster University, Lancaster, UK

Abstract We present Super Dual Auroral Radar Network observations of ionospheric convection during substorms. Substorms were grouped according to their onset latitude, onset magnetic local time, and the prevailing sense of interplanetary magnetic field (IMF) B_Y. The radar observations were then sorted according to substorm group and average convection patterns produced. Here we discuss the patterns corresponding to substorms with onsets occurring in the 65°–67° onset latitude range, at either early (20–22 h) or late (01–03 h) magnetic local times, during intervals of either dominant positive or negative IMF B_Y. We show that the morphology of the convection patterns differs from that predicted by existing empirical models, with the location of the nightside convection throat being largely consistent with the location of substorm onset. The expected IMF B_Y-induced dawn-dusk convection asymmetry can be enhanced on the nightside when the substorm onset occurs at a fortuitous location but can equally be removed or even reversed from this expected state. Thus, the nightside convection asymmetries are seemingly unrelated to the instantaneous sense of IMF B_Y.

Plain Language Summary One of the main drivers of the aurora, or northern lights, is a phenomenon called the "magnetospheric substorm." Substorms deposit large amounts of energy into the atmosphere, affecting the flow of plasma—an electrically charged gas—high up in the atmosphere, and producing various "space weather" effects that can disrupt radio communications, satellite orbits, and GPS transmissions. Substorms occur on the nightside of the planet, at a variety of local times from 2100 to 0300 h and their effect on the plasma flow is correspondingly variable. In this paper, we show what form the atmospheric plasma flows take during substorms occurring at different local times. We conclude that clear differences in the flows associated with substorms at different local times are apparent. These effects are distinct from those currently included in geophysics models.

1. Introduction

The morphology of the ionospheric convection pattern is governed by the superposition of flows driven independently by dayside coupling processes (e.g., magnetopause reconnection) and by internal magnetospheric dynamics such as substorms (e.g., Lockwood et al., 1990). It is well documented that in the case of dayside driving, the B_Y component of the interplanetary magnetic field (IMF) introduces asymmetries into the coupled solar wind-magnetosphere-ionosphere system (Haaland et al., 2017, and references therein). In the Northern Hemisphere ionosphere, the generally accepted form of this asymmetry is that when IMF B_Y is positive, a round cell is formed at dusk and a crescent cell at dawn, with this asymmetry being reversed when B_Y is negative (e.g., Lockwood, 1991), or when considering the equivalent Southern Hemisphere flows (e.g., Cowley et al., 1991). In reality, asymmetries between the dawn and dusk cells may be manifest in a wide range of characteristics such as their relative size, strength, orientation and shape (e.g., Grocott et al., 2012; Pettigrew et al., 2010; Ruohoniemi & Greenwald, 2005). Ultimately, the morphology at any given time will be governed by a combination of IMF B_Y, dipole tilt angle (e.g., Pettigrew et al., 2010) and the effects of internal magnetotail driving (e.g., Grocott, 2017).

Substorms are already known to influence the ionospheric convection in ways that will produce asymmetries. Weimer (1999, 2001, 2005), for example, used Dynamics Explorer 2 spacecraft observations of the ionospheric electric field to reveal that the Harang discontinuity (Maynard, 1974) was considerably more pronounced when substorms were in progress. Provan et al. (2004) and Bristow and Jensen (2007) used Super Dual Auroral

Radar Network (SuperDARN) observations to show that enhanced flows were present outside of the flow suppression region that occurs due to the high conductivities produced at substorm onset (e.g., Grocott et al., 2009; Kirkwood et al., 1988). This effect naturally results in a dawn-dusk asymmetry about the onset location, which tends to occur in the premidnight sector at an average local time of 23 h (e.g., Frey et al., 2004). This raises the question of whether solar wind driving or internal driving by magnetospheric substorms will govern the instantaneous asymmetry in the convection pattern. In addition, as noted by Weimer (2005), there remains the question of whether the ionosphere responds to IMF changes at the same rate at different magnetic local time (MLT) locations. Even if the IMF is ultimately responsible for the nightside asymmetries, they will thus need to be treated independently.

Limited evidence has been presented to determine the relative influence of IMF B_Y and substorm electrodynamics on dawn-dusk asymmetries in the ionospheric convection pattern. Weimer (1999, 2001, 2005) did not discriminate between substorm onset location when deriving substorm-time convection patterns and Bristow and Jensen (2007) selected substorms with similar onset locations. Provan et al. (2004) transformed their observations into a substorm-oriented coordinate system, thus removing any asymmetries due directly to substorms. They were nevertheless able to discern a dawn-dusk asymmetry in the strength of the nightside flows, which they attributed to the prevailing IMF B_Y conditions. In a set of case studies, Liou and Ruohoniemi (2006a, 2006b) also suggested that the evolution of the substorm expansion was linked to the IMF B_Y-driven dawn-dusk convection asymmetry. These studies thus suggest that the substorm-related convection asymmetry is controlled by IMF B_Y. A series of case studies by Bristow et al. (2001, 2003), on the other hand, suggested that the convection evolved in direct response to the substorm onset, with the "convection throat" (the gap between the dawn and dusk convection cells where they diverge from equatorward to sunward) moving to the onset location. Grocott et al. (2010) looked explicitly at the convection evolution during substorms that occurred during IMF B_Y-dominated intervals and confirmed that, following onset, any prior B_Y-associated dawn-dusk asymmetry was eroded. In their case, the B_Y asymmetry was replaced by a more traditional Harang asymmetry.

Given these somewhat varied conclusions, the aim of this paper is to demonstrate the dominant large-scale relationship between substorm onset location and the morphology of the ionospheric convection pattern. We thus present average ionospheric patterns derived from SuperDARN radar observations of the Northern and Southern Hemispheres, for substorm intervals of positive and negative IMF B_Y, where the substorm onsets were observed at atypically early (20–22 h) or late (01–03 h) magnetic local times. In this way we can isolate any asymmetries associated with IMF B_Y from those associated with the substorm onsets. We find that the patterns differ from those derived when considering only IMF or dipole tilt angle dependences. In particular, and in agreement with Bristow et al. (2001, 2003), the local time of the nightside convection throat is revealed to closely agree with the local time of the substorm onset. We therefore conclude that to correctly represent the ionospheric convection pattern, empirical models are required that can better account for magnetotail dynamics than simple IMF binning, or binary substorm and nonsubstorm classifications.

2. Methodology

We have used a similar methodology to that employed by Grocott et al. (2010) to produce averaged ionospheric convection patterns for different substorm onset MLTs and IMF B_Y conditions. In summary, we have used data from the IMAGE satellite (Frey et al., 2004) to derive a list of isolated Northern Hemisphere substorms, that is, substorms where at least 2 h has passed since the previous onset. Our list was then filtered by substorm onset latitude, which is necessary owing to the strong relationship between onset latitude and convection morphology (e.g., Bristow, 2009; Grocott et al., 2009). For our study, we chose to include only substorms with onset latitudes between 65° and 67° magnetic. This range was chosen because (a) substorms need to be of sufficiently high latitude to be well observed by the latitudinally restricted fields of view of the SuperDARN radars and (b) the lowest latitude end of the range satisfying (a) will be of the highest intensity (Milan et al., 2009) and therefore likely to produce the strongest observable effects in the ionosphere.

This set of events was then further subdivided based on the magnetic local time of the substorm onsets, with only those occurring at an atypically early or late MLT being selected. We define early onsets as those occurring within the range 20–22 MLT and late onsets within 01–03 MLT. We note that this is not symmetrical about midnight, with the typical onset MLT being somewhat early itself at ~23 MLT in our data set (with a mean and standard deviation of 22.9 h and 1.3 h, respectively). Observations from the Advanced Composition Explorer

(ACE) spacecraft (Smith et al., 1998) were then used to reduce our substorm sets to only those where B_Y was either less than −2 nT or greater than +2 nT. This was done by first time lagging the IMF data from ACE to the dayside ionosphere according to the method of Khan and Cowley (1999) and then determining a set of IMF B_Y averages, from 60 min before to 20 min after each substorm onset. We chose this time interval for the IMF averages to allow for (a) any B_Y effects to propagate across the dayside and polar cap ionosphere, (b) a given state of B_Y to remain until 10 min into the substorm expansion phase, and (c) an uncertainty of a further 10 min in the time-lag calculation (Khan & Cowley, 1999). The resulting number of substorm intervals contributing to each of the four categories is 24 ($B_Y < 0$/early), 46 ($B_Y > 0$/early), 29 ($B_Y < 0$/late), 8 ($B_Y > 0$/late). We note that the last of our categories contains a relatively small number of substorms and the possible ramifications of this are discussed in section 3.

Eight sets of ionospheric convection velocity vectors were then compiled from the Super Dual Auroral Radar Network (SuperDARN) (Chisham et al., 2007) archive, for each of the two IMF B_Y bins, two onset MLT bins, and two hemispheres. Average convection patterns were then derived by applying the global Map Potential fitting algorithm (Ruohoniemi & Baker, 1998; Shepherd & Ruohoniemi, 2000) to a superposition of the data from the 10 min following substorm onset. We use a 10 min average to increase the amount of data in each set and remove short-timescale variations in the patterns. The number of radar vectors contributing to each average varies between 297 and 1641, and the significance of this is discussed further below. In deriving the Southern Hemisphere convection patterns we use the same set of Northern Hemisphere substorm observations and contemporaneous radar data from the south. We then estimate the southern onset MLTs using the result of Østgaard et al. (2004) which provides the expected offset in MLT between the northern and southern auroral onsets. This offset is given by $\Delta\text{MLT(h)} = -0.017\theta + 3.44$, where θ is the IMF clock angle (in degrees) and ΔMLT is positive for a southern onset location dawnward of the northern location. We note that in deriving this equation Østgaard et al. (2004) used only 12 events, all of which were observed premidnight in MLT. Although this is not ideal, it is advantageous for our purposes to compare contemporaneous convection data from both hemispheres. Hence, we cannot use Southern Hemisphere substorm onsets to derive the Southern Hemisphere convection patterns as these would be independent of their northern counterparts. We therefore show the predicted Southern Hemisphere onset MLT for information but weight our interpretation in the following sections accordingly.

To aid interpretation of our results, we also produce a set of average (Northern Hemisphere) convection patterns with no discrimination based on substorm occurrence. In this case we use the same year range (2000–2004) and filter the data by the same IMF B_Y conditions used in the substorm analysis (<−2 nT or >+2 nT). Pettigrew et al. (2010) found modest variations in the nightside convection under different dipole tilt angles, so we also filter by dipole tilt angle (<−10° or > +10°, the same tilt ranges used by Pettigrew et al., 2010) in order to determine whether any aspects of our substorm convection patterns might be attributed to dipole tilt.

3. Results

Figure 1 presents the results of our dipole tilt angle analysis. Two pairs of average convection patterns are shown for each of the two IMF B_Y directions. The $B_Y < 0$ maps are shown on the left and the $B_Y > 0$ maps are shown on the right. Figures 1a and 1b present the results for negative tilt and Figures 1c and 1d for positive tilt. Each map is presented such that noon is to the top and dusk to the left. Solid (dashed) contours show negative (positive) electric potential, with the outer contours at ±3 kV and subsequent contours at intervals of 6 kV. The dotted circles are concentric lines of magnetic latitude from 60° to the pole and in all cases the view is down onto the Northern Hemisphere (such that in the case of Southern Hemisphere data, the view is through the Earth). The gray outline indicates the Heppner-Maynard boundary of the convection patterns (Shepherd & Ruohoniemi, 2000). The icon in the top right of each panel shows the averaged IMF clock angle vector in the GSM *y-z* plane and the icon in the bottom right shows the average dipole tilt angle. These patterns reveal similar characteristics to previous studies of the IMF dependence of the convection (e.g., Ruohoniemi & Greenwald, 2005) and only a modest dependence on tilt angle which is similar to, although perhaps slightly less pronounced than, the results of Pettigrew et al. (2010). It is worth noting that in three out of the four cases, the nightside convection throat is premidnight, consistent with the typical local time of substorm onset. This is considered further below.

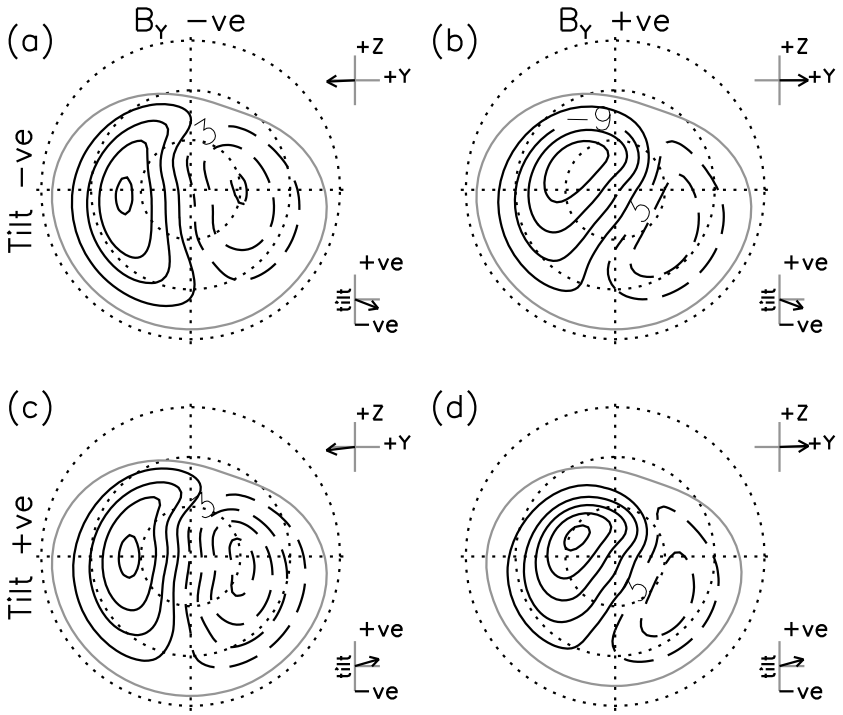

Figure 1. Average Northern Hemisphere contour maps of the ionospheric electric potential for IMF (a, c) B_Y negative and (b, d) B_Y positive for negative dipole tilt intervals (Figures 1a and 1b) and positive dipole tilt intervals (Figures 1c and 1d). In each map, noon is to the top and dusk to the left. Solid (dashed) contours show negative (positive) electric potential, with the outer contours at ±3 kV and subsequent contours at intervals of 6 kV. The dotted circles are concentric lines of magnetic latitude from 60° to the pole, and in all cases the view is down onto the Northern Hemisphere (such that in (e) the view is through the Earth). The gray outline shows the equatorward convection boundary. The icon in the top right of each panel shows the averaged IMF clock angle vector in the GSM *y*-*z* plane, and the icon in the bottom right shows the average dipole tilt angle.

Figure 2 presents the average patterns for the substorm intervals, presented in a similar format to Figure 1. Here the two columns again correspond to the two senses of IMF B_Y, with the rows corresponding to groupings of substorm onset MLT and hemisphere. In this case we have included *a*+ symbol on each panel indicating the average location of substorm onset (or predicted location in the case of the Southern Hemisphere maps). In addition, owing to the vastly reduced statistics in comparison to Figure 1, we also include information on the number of gridded radar vectors (Ruohoniemi & Greenwald, 2005) that contributed to the global fit in each case. The gray dots on each panel indicate the spatial distribution of the vectors, with the total number shown beneath each panel. This enables us to gauge the reliability of the patterns whereby, loosely speaking, a region with fewer measurements is likely to produce a poorer representation of the convection pattern. Only Figure 2h appears to strongly suffer from reduced data coverage. This is likely to be due to a combination of the reduced number of substorms in this B_Y-onset MLT group, and the lower number of SuperDARN radars in the Southern Hemisphere. We comment further on the significance of this, below.

Figures 2a–2d show convection patterns for substorms with onsets in the early MLT category and Figures 2e–2h show the late MLT category. A number of general observations can be made. First, in each case, the convection morphology on the dayside and in the polar cap largely resembles that in Figure 1. In other words, the IMF categorization is here producing the expected round and crescent shapes with all Northern Hemisphere B_Y negative patterns (a,e) and Southern Hemisphere B_Y positive patterns (d,h) having the more crescent shaped cell in the postnoon sector, and all Northern Hemisphere B_Y positive patterns (b,f) and Southern Hemisphere B_Y negative patterns (c,g) having the more crescent shaped cell in the prenoon sector. More interestingly, the nightside convection morphologies do not all exhibit the expected dusk-dawn or interhemispheric asymmetries. Instead, there is a general trend for any convection asymmetry to be related to the substorm onset location. This is considered further, below.

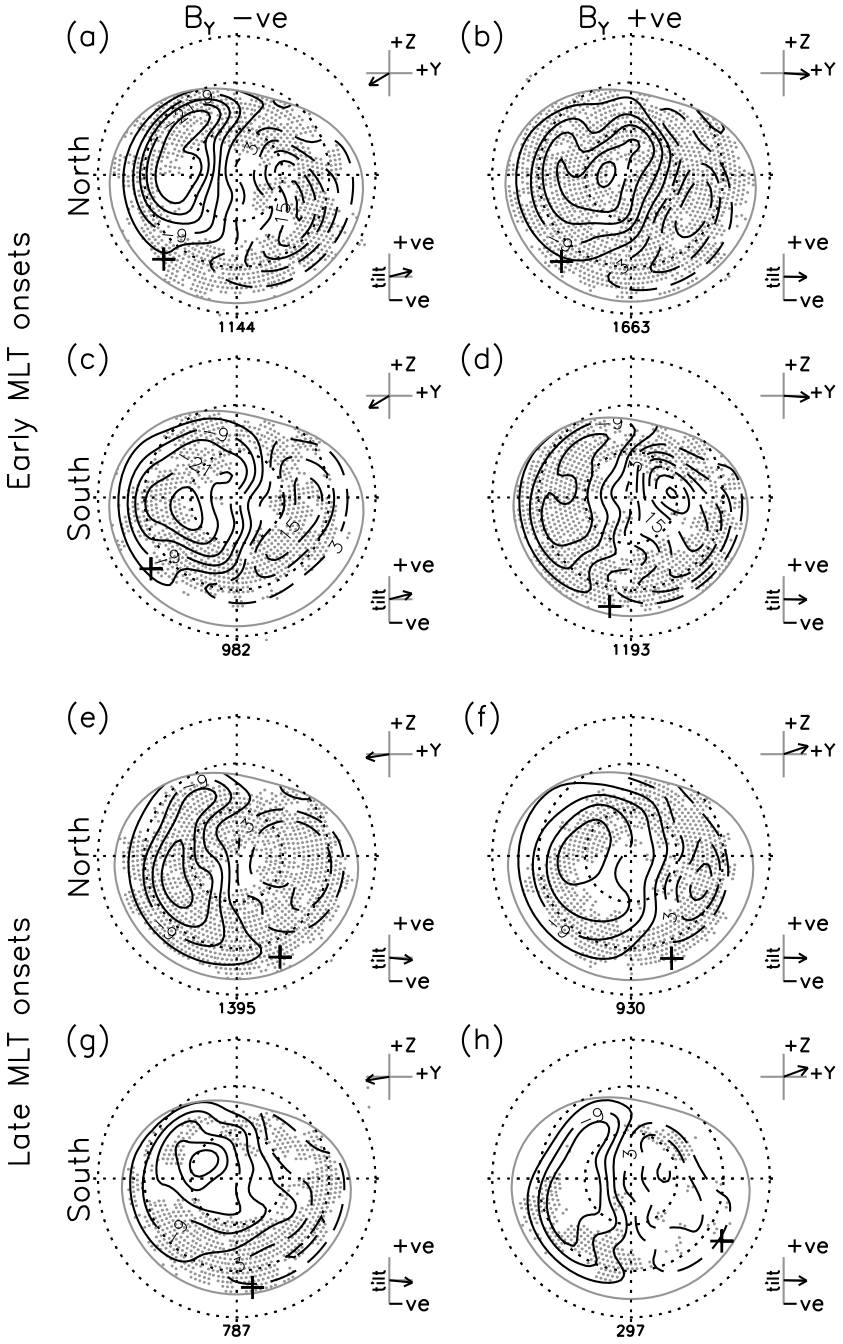

Figure 2. Average contour maps of the Northern and Southern Hemisphere ionospheric electric potential for substorm intervals, in a similar format to Figure 1. On each panel, the + symbol indicates the average location of substorm onset (or predicted location in the case of the Southern Hemisphere maps). The gray dots indicate where SuperDARN flow vectors were present in the global fitting analysis, with the total number of vectors indicated beneath each panel. Patterns are presented for (a–d) early MLT substorms and for (e–h) late MLT substorms.

Consider the pattern in Figure 2a. In this case, the negative sense of B_Y has produced a dayside convection morphology that exhibits a crescent shape at dusk, with flows that have a corresponding anticlockwise sense into the polar cap from the dayside. On the nightside, however, "crescent" would better describe the dawn cell, with the flows out of the polar cap now rotating in an clockwise direction, toward the premidnight sector, such that the nightside convection throat lies close to the onset location. In contrast, the B_Y positive pattern in Figure 2b has a nightside component that seems more consistent with the expected B_Y dawn-dusk asymmetry, accentuating the crescent shape of the dawn cell. This has the effect of bringing the nightside component of

the average pattern more in line with the theoretical round and crescent cell picture discussed above, that is largely suppressed in the nightside portions of the average patterns in Figure 1. We suggest that this latter effect is because the patterns in Figure 1 are unconstrained by substorm activity and are thus likely to contain data from all phases of the substorm cycle and from substorms occurring at a variety of local times. Overall, these results reveal nightside convection morphologies (in Figures 2a and 2b) that are largely the same, which is not what we would expect if the dawn-dusk asymmetry was a result of opposite IMF B_Y control.

In Figures 2c and 2d we show examples of the Southern Hemisphere convection pattern. Recall that these have been derived from Southern Hemisphere SuperDARN observations that are contemporaneous with the Northern Hemisphere data used to produce the patterns in Figures 2a and 2b. Consider first Figure 2c, which shows the southern counterpart to the pattern in Figure 2a. Being derived from simultaneous intervals, the patterns are expected to exhibit the opposite B_Y-associated dusk-dawn asymmetry. While this is true of the dayside flows, it is not true on the nightside, where the flows instead appear to have a very similar morphology. This is consistent with the substorm onset location being early in MLT in both cases. In the Southern Hemisphere case the nightside convection throat does not match quite as closely with the predicted average onset location. This could be due to data coverage, which is slightly limited in the equatormost part of the nightside region close to the onset location and nightside convection throat. It could also be attributed to uncertainty in the Østgaard et al. (2004) predictions as noted in section 2. Nevertheless, the dawn-dusk asymmetry present in these two patterns is still broadly consistent, with the key result being that it exhibits the same sense in both hemispheres.

The morphology of the convection in Figure 2d is slightly different but still fully consistent with the above discussion. In this case, the interhemispheric offset between the northern and southern onset MLTs serves to move the southern onset closer to magnetic midnight. This appears to be related to the dusk cell reversing more sharply in the premidnight sector, but the dawn cell protrusion across midnight from dawn to dusk is largely the same as in Figures 2a–2c. The day-night asymmetry in Figure 2d is similar to that observed in Figure 2a, with the dayside flows exhibiting the expected B_Y-associated dawn-dusk asymmetry and the nightside flows the opposite. Overall, these results serve to illustrate that the Southern Hemisphere patterns do not exhibit a dawn-dusk mirror symmetry with respect to the north, much like Østgaard et al. (2004, 2011) found of the onset locations. Instead, their morphologies appear to be related to the substorm process, with the convection throat located close to the substorm onset location.

Turning now to the Northern Hemisphere patterns for the late MLT onsets shown in Figures 2e and 2f, we find a somewhat different result. Here the patterns appear to exhibit the expected B_Y-associated dawn-dusk asymmetry on both the dayside and nightside, with the crescent cell at dusk for B_Y negative and at dawn for B_Y positive. However, there are additional differences in the dawn-dusk asymmetry that appear to relate to the substorm onset. The protrusion across the midnight sectors of the dusk cell in Figure 2e, for example, is much more apparent than in either of the B_Y-negative patterns in Figure 1. This accentuates the crescent and round cell shapes in a similar (but mirrored) way to the pattern in Figure 2b. Comparing this result with the pattern in Figure 2a which, based on IMF B_Y considerations alone ought to be the same, we find the morphology of the nightside convection to be dramatically different. The dayside morphology, on the other hand, remains as expected for B_Y negative, albeit with a dayside throat location at an earlier MLT. This appears to be related to a modest rotation of the pattern as whole and may be a result of the dipole tilt angle, which is positive in Figure 2a compared to slightly negative in Figure 2e, and is broadly consistent with the behavior of the patterns in Figure 1. The difference in the nightside morphology, on the other hand, cannot be similarly explained by dipole tilt and instead appears to be again related to the MLT of substorm onset.

In Figure 2f, although the dawn-dusk asymmetry is opposite in sense to that in Figure 2e, it takes a very different form. Rather than the crescent cell (the dawn cell, in this case) protruding across the midnight sector, it has retreated toward dawn. Thus, we have a small dawn cell and a large dusk cell, in common with the pattern in Figure 2e. The net result of this is that the nightside convection throat is postmidnight in both cases, coinciding with the location of substorm onset in each case. If we now compare this pattern to that in Figure 2b we again see two different nightside convection morphologies. Although the overall sense of the dawn-dusk asymmetries is the same in this case, consistent with a positive IMF B_Y, the nightside portion of the pattern is dominated by the dawn cell in Figure 2b and by the dusk cell in Figure 2f. This gives a nightside convection throat in Figure 2f that is displaced by ~3 h of MLT with respect to its Figure 2b counterpart, despite both occurring for similar B_Y and dipole tilt angle conditions.

Finally, we consider the results in Figures 2g–2h, which provide the southern counterparts to the northern patterns in Figures 2e and 2f. We are forced to disregard the results in Figure 2h since the coverage of radar data is poor, particularly in the vicinity of substorm onset, such that little can be concluded about the convection in this case. The pattern shown in Figure 2g, on the other hand, is still reasonably well constrained by the data. In this case, the nightside convection throat does not match as well with the predicted onset location, although we note that the Østgaard et al. (2004) prediction may not be valid for postmidnight onsets, as discussed in section 2. The nightside pattern in this case could reasonably be considered to exhibit mirror dawn-dusk asymmetry with respect to its northern counterpart in Figure 2e. If the north-south asymmetry was slightly greater than the Østgaard et al. (2004) prediction, then the southern onset would in fact be premidnight and might explain the morphology of the nightside flows resembling those in Figure 2b. It is worth noting that Milan et al. (2010) suggested a larger north-south asymmetry might exist for the extremes of onset MLT, which would be consistent with the results in Figures 2a and 2g although we have no direct evidence with which to support such a hypothesis.

4. Discussion

Overall, our results serve to illustrate that in order to better capture the different characteristic ionospheric convection morphologies in empirical models, we need to include some quantification of magnetospheric dawn-dusk asymmetry in addition to the currently used IMF and dipole tilt classifications. Our results suggest that substorm onset location may provide a suitable parameter by which to classify nightside convection asymmetries. A number of previous studies have found that the typical location for substorm onset is in the premidnight sector at ~23 MLT, which is also where the typical nightside convection throat is found (e.g., Ruohoniemi & Greenwald, 2005). Lu et al. (2016) suggest that this fundamental dawn-dusk asymmetry is caused by the Hall effect which is stronger on the duskside due to the higher ion temperature, thinner current sheet, and smaller normal magnetic field. Other studies have found that owing to the growth of the Harang discontinuity during the substorm expansion phase, the nightside throat moves postmidnight (e.g., Grocott et al., 2006, 2009; Weimer, 2005). This is not unexpected and has been shown to be related to the development of the subauroral polarization streams (Foster & Vo, 2002). We explicitly focus on the onset and early expansion phase as we are interested in what produces the initial dawn-dusk asymmetry, rather than those that develop later in the substorm process.

It is presumably during the growth phase that the magnetospheric asymmetry responsible for the substorm onset location and associated nightside convection morphology first starts to develop. This would be consistent with the work of Tenfjord et al. (2017), who demonstrate that a modest dawn-dusk asymmetry can be introduced into the nightside magnetosphere over the course of a few tens of minutes as a direct result of dayside reconnection with a B_Y-dominated IMF. On the other hand, while Østgaard et al. (2004) predict a B_Y-associated north-south local time offset, Østgaard et al. (2011) demonstrate only a very weak relationship between B_Y and the actual local time of onset in a given hemisphere. Milan et al. (2010) suggested an explanation for this is that for atypically early and late substorm onsets it may take a number of growth phases for large asymmetries to be introduced. This would then introduce a significant time dependence to the nightside dawn-dusk asymmetry that cannot be captured by a simple IMF classification. This is consistent with the work of Grocott and Milan (2014) who showed that longer (>6 h) intervals of steady B_Y can continue to enhance dawn-dusk asymmetries in the nightside convection, although it is worth noting that in their study it was under northward, but B_Y-dominated IMF conditions that larger asymmetries became apparent.

If the mechanism responsible for the local time of substorm onset takes effect in the magnetotail during the growth phase, then one might expect to find the associated dawn-dusk convection asymmetry also developing during the growth phase. There is some evidence that the nightside convection starts to respond during this time (e.g., Bristow & Jensen, 2007) but, having examined both the growth phase and expansion phase flows during our superposed substorm intervals, we find that the clearest asymmetries appear following substorm onset. This is consistent with the nightside ionospheric flows being driven largely by magnetotail reconnection (Cowley & Lockwood, 1996), such that only after reconnection commences at (or shortly after) onset are the flows reorganized according to the state of the magnetosphere at that time. Nishimura and Lyons (2016) showed that localized reconnection can be triggered in the tail by lobe flow channels which may develop over a wide range of local times. Work by, for example, Østgaard et al. (2011) suggests that subsequently, any interhemispheric dusk-dawn asymmetry will begin to decrease as the flows of newly reconnected closed flux act to restore symmetry (Reistad et al., 2016). This would suggest that the asymmetry

develops during the growth phase, peaks after onset, and then decays, and would explain why we find clear dawn-dusk asymmetries in the nightside convection during the early expansion phase.

It is worth noting that other studies have not revealed the same result as our work. Zou et al. (2009), for example, found that substorm onset starts within the Harang, not within the convection throat region. A number of possible explanations could exist for this apparent discrepancy. Their study included lower latitude substorms, which tend to be more intense (Milan et al., 2009) and thus produce larger conductivity enhancements in the ionosphere. It is known that enhanced conductivities can have a significant impact on the convection (e.g., Grocott et al., 2009; Kirkwood et al., 1988) and thus may produce a more complicated effect than that revealed here. In addition, the SuperDARN fields of view during the lifetime of the IMAGE satellite did not extend below ~60° magnetic latitude and thus were not ideally located to monitor the equatormost edge of the convection zone. Ideally, we would repeat this study using more recent data taken by the midlatitude extension to SuperDARN, for substorms observed simultaneously in both hemispheres. Unfortunately, such an undertaking is hampered by the lack of any contemporaneous observations from midlatitude SuperDARN radars and interhemispheric global auroral imagery. Other substorm identification methods using ground-based auroral imagers (e.g., Zou et al., 2010) and magnetometers (e.g., Forsyth et al., 2015) have been developed that may be able to mitigate this issue to some extent, but it remains a challenge to study large-scale ionospheric dynamics with spatially limited observations.

Lastly, it is apparent that the strength of the convection cells is also generally asymmetric between dawn and dusk and between hemispheres. It is worth considering whether there is any pattern to these asymmetries that might shed further light on the mechanism that effects the changes in morphology. An inspection of the strength of the convection cells provided by our analysis reveals no obvious relationship with the onset local time, although we note that this result may be influenced by a number of factors. Asymmetries in the convection cell strength have previously been associated with reconnection of overdraped lobe field lines with the dawnside or duskside closed flankside field lines (Watanabe et al., 2007) and day-night conductivity gradients (e.g., Lyatsky et al., 1974; Ridley et al., 2004). Pettigrew et al. (2010) also noted that nonuniform radar data coverage might play a role, as could the nondipolar, asymmetric nature of the Earth's magnetic field. Such a range of possible sources of asymmetry in convection cell strength makes isolating any possible effect of substorm onset local time nontrivial. We thus leave further consideration of this aspect of the asymmetry to future studies.

5. Summary

In this paper we have presented maps of the average ionospheric convection morphology for different conditions of IMF orientation and substorm onset location. This is in contrast to current empirical models which characterize the convection only by parameters such as IMF orientation and strength, dipole tilt angle, or whether or not a substorm is in progress. None of these existing models take into account how asymmetries in the convection are associated with the local time of substorm onset. Our results show that both IMF B_Y and substorm onset local time appear to be associated with morphological features in the convection pattern, with the nightside component of the convection much more sensitive to onset location than to IMF B_Y. This is evident in two ways: (a) the lack of expected B_Y control which can be seen by comparing, for example, Figures 2a and 2b, which occur under similar B_Y conditions yet have distinctly different nightside convection patterns and (b) the lack of interhemispheric asymmetry which can be seen by comparing, for example, Figures 2a and 2c, which ought to exhibit the opposite B_Y-associated dawn-dusk asymmetry yet in the nightside show almost identical morphology. With no direct relationship between substorm onset local time and IMF B_Y, both therefore need to be considered independently to better characterize the different convection morphologies that exist.

Acknowledgments
The authors wish to thank the PI groups of the SuperDARN consortium for provision of the radar data. SuperDARN is funded by the research agencies of Australia, China, Canada, France, Italy, Japan, Norway, South Africa, the U.K., and the U.S. SuperDARN data are freely provided for scientific research purposes and can be obtained by contacting the corresponding author or any of the SuperDARN PI research groups, as detailed at http://www.superdarn.ac.uk.
A. G. was supported to conduct this work by NERC grant NE/P001556/1.
H. J. L. was supported by a Lancaster University FST research studentship.
A. G. is grateful to A. B. B. Grocott for useful, if one-sided, discussions.

References

Bristow, W. A. (2009). Relationship between substorm onset locations and nightside convection pattern features. *Journal of Geophysical Research*, *114*, A12202. https://doi.org/10.1029/2009JA014576

Bristow, W. A., & Jensen, P. (2007). A superposed epoch study of SuperDARN convection observations during substorms. *Journal of Geophysical Research*, *112*, A06232. https://doi.org/10.1029/2006JA012049

Bristow, W. A., Otto, A., & Lummerzheim, D. (2001). Substorm convection patterns observed by the super dual auroral radar network. *Journal of Geophysical Research*, *106*, 24,593 – 24,609.

Bristow, W. A., Sofko, G. J., Stenbaek-Nielsen, H. C., Wei, S., Lummerzheim, D., & Otto, A. (2003). Detailed analysis of substorm observations using SuperDARN, UVI, ground-based magnetometers, and all-sky imagers. *Journal of Geophysical Research*, *108*(A3), 1124. https://doi.org/10.1029/2002JA009242

Chisham, G., Lester, M., Milan, S. E., Freeman, M. P., Bristow, W. A., Grocott, A., … Walker, A. D. M. (2007). A decade of the Super Dual Auroral Radar Network (SuperDARN): Scientific achievements, new techniques and future directions. *Surveys in Geophysics*, *28*, 33–109. https://doi.org/10.1007/s10712-007-9017-8

Cowley, S. W. H., & Lockwood, M. (1996). Time-dependent flows in the coupled solar wind-magnetosphere-ionosphere system. *Advances in Space Research*, *18*, 141–150.

Cowley, S. W. H., Morelli, J. P., & Lockwood, M. (1991). Dependence of convective flows and particle precipitation in the high-latitude dayside ionosphere on the x and y components of the interplanetary magnetic field. *Journal of Geophysical Research*, *96*(A4), 5557–5564.

Forsyth, C., Rae, I. J., Coxon, J. C., Freeman, M. P., Jackman, C. M., Gjerloev, J., & Fazakerley, A. N. (2015). A new technique for determining Substorm Onsets and Phases from Indices of the Electrojet (SOPHIE). *Journal of Geophysical Research: Space Physics*, *120*, 10,592–10,606. https://doi.org/10.1002/2015JA021343

Foster, J. C., & Vo, H. B. (2002). Average characteristics and activity dependence of the subauroral polarization stream. *Journal of Geophysical Research*, *107*(A12), 1475. https://doi.org/10.1029/2002JA009409

Frey, H. U., Mende, S. B., Angelopoulos, V., & Donovan, E. F. (2004). Substorm onset observations by IMAGE-FUV. *Journal of Geophysical Research*, *109*, A10304. https://doi.org/10.1029/2004JA010607

Grocott, A. (2017). Time-dependence of dawn-dusk asymmetries in the terrestrial ionospheric convection pattern. In S. E. Haaland, A. Runov, & C. Forsyth (Eds.), *Dawn-dusk asymmetries in planetary plasma environments* (Vol. 228). Hoboken, NJ: American Geophysical Union Monograph. https://doi.org/10.1002/9781119216346.ch9

Grocott, A., Lester, M., Parkinson, M. L., Yeoman, T. K., Dyson, P. L., Devlin, J. C., & Frey, H. U. (2006). Towards a synthesis of substorm electrodynamics: HF radar and auroral observations. *Annales Geophysicae*, *24*, 3365–3381.

Grocott, A., & Milan, S. E. (2014). The influence of IMF clock angle timescales on the morphology of ionospheric convection. *Journal of Geophysical Research: Space Physics*, *119*, 5861–5876. https://doi.org/10.1002/2014JA020136

Grocott, A., Milan, S. E., Imber, S. M., Lester, M., & Yeoman, T. K. (2012). A quantitative deconstruction of the morphology of high-latitude ionospheric convection. *Journal of Geophysical Research*, *117*, A05317. https://doi.org/10.1029/2012JA017580

Grocott, A., Milan, S. E., Sato, N., Wild, J. A., Yeoman, T. K., & Yukimatu, A. S. (2010). Superposed epoch analysis of the ionospheric convection evolution during substorms: IMF B_Y dependence. *Journal of Geophysical Research*, *115*, A00I06. https://doi.org/10.1029/2010JA015728

Grocott, A., Wild, J. A., Milan, S. E., & Yeoman, T. K. (2009). Superposed epoch analysis of the ionospheric convection evolution during substorms: Onset latitude dependence. *Annales Geophysicae*, *27*(2), 591–600.

Haaland, S. E., Runov, A., & Forsyth, C. (2017). *Dawn-dusk asymmetries in planetary plasma environments, Geophysical Monograph Series*. Hoboken, NJ: John Wiley.

Khan, H., & Cowley, S. W. H. (1999). Observations of the response time of high-latitude ionospheric convection to variations in the interplanetary magnetic field using EISCAT and IMP-8 data. *Annales Geophysicae*, *17*, 1306–1335. https://doi.org/10.1007/s005850050858

Kirkwood, S., Opgenoorth, H. J., & Murphree, J. S. (1988). Ionospheric conductivities, electric-fields and currents associated with auroral substorms measured by the EISCAT radar. *Planetary and Space Science*, *36*(12), 1359–1380.

Liou, K., & Ruohoniemi, J. (2006a). A case study of relationship between substorm expansion and global plasma convection. *Geophysical Research Letters*, *33*, L02105. https://doi.org/10.1029/2005GL024736

Liou, K., & Ruohoniemi, J. (2006b). Correction to "A case study of relationship between substorm expansion and global plasma convection". *Geophysical Research Letters*, *33*, L10101. https://doi.org/10.1029/2005GL024736

Lockwood, M. (1991). Modelling the high-latitude ionosphere. In *Proceedings IEE Colloqium on 'National Radio Propagation Programme' 10*. London, UK: IEE.

Lockwood, M., Cowley, S. W. H., & Freeman, M. P. (1990). The excitation of plasma convection in the high-latitude ionosphere. *Journal of Geophysical Research*, *95*, 7961–7972. https://doi.org/10.1029/JA095iA06p07961

Lu, S., Lin, Y., Angelopoulos, V., Artemyev, A. V., Pritchett, P. L., Lu, Q., & Wang, X. Y. (2016). Hall effect control of magnetotail dawn-dusk asymmetry: A three-dimensional global hybrid simulation. *Journal of Geophysical Research: Space Physics*, *121*, 11,882–11,895. https://doi.org/10.1002/2016JA023325

Lyatsky, W. B., Maltsev, Y. P., & Leontyev, S. V. (1974). Three-dimensional current system in different phases of a substorm. *Planetary and Space Science*, *22*(8), 1231–1247. https://doi.org/10.1016/0032-0633(74)90007-5

Maynard, N. C. (1974). Electric-field measurements across Harang discontinuity. *Journal of Geophysical Research*, *79*(31), 4620–4631.

Milan, S. E., Grocott, A., Forsyth, C., Imber, S. M., Boakes, P. D., & Hubert, B. (2009). A superposed epoch analysis of auroral evolution during substorm growth, onset and recovery: Open magnetic flux control of substorm intensity. *Annales Geophysicae*, *27*(2), 659–668.

Milan, S. E., Grocott, A., & Hubert, B. (2010). A superposed epoch analysis of auroral evolution during substorms: Local time of onset region. *Journal of Geophysical Research*, *115*, A00I04. https://doi.org/10.1029/2010JA015663

Nishimura, Y., & Lyons, L. R. (2016). Localized reconnection in the magnetotail driven by lobe flow channels: Global MHD simulation. *Journal of Geophysical Research: Space Physics*, *121*, 1327–1338. https://doi.org/10.1002/2015JA022128

Østgaard, N., Laundal, K. M., Juusola, L., Åsnes, A., Haaland, S. E., & Weygand, J. M. (2011). Interhemispherical asymmetry of substorm onset locations and the interplanetary magnetic field. *Geophysical Research Letters*, *38*, L08104. https://doi.org/10.1029/2011GL046767

Østgaard, N., Mende, S. B., Frey, H. U., Immel, T. J., Frank, L. A., Sigwarth, J. B., & Stubbs, T. J. (2004). Interplanetary magnetic field control of the location of substorm onset and auroral features in the conjugate hemispheres. *Journal of Geophysical Research*, *109*, A07204. https://doi.org/10.1029/2003JA010370

Pettigrew, E. D., Shepherd, S. G., & Ruohoniemi, J. M. (2010). Climatological patterns of high-latitude convection in the Northern and Southern Hemispheres: Dipole tilt dependencies and interhemispheric comparisons. *Journal of Geophysical Research*, *115*, A07305. https://doi.org/10.1029/2009JA014956

Provan, G., Lester, M., Mende, S., & Milan, S. (2004). Statistical study of high-latitude plasma flow during magnetospheric substorms. *Annales Geophysicae*, *22*, 3607–3624.

Reistad, J. P., Østgaard, N., Tenfjord, P., Laundal, K. M., Snekvik, K., Haaland, S., … Grocott, A. (2016). Dynamic effects of restoring footpoint symmetry on closed magnetic field lines. *Journal of Geophysical Research: Space Physics*, *121*, 3963–3977. https://doi.org/10.1002/2015JA022058

Ridley, A. J., Gombosi, T. I., & DeZeeuw, D. L. (2004). Ionospheric control of the magnetosphere: Conductance. *Annales Geophysicae*, *22*(2), 567–584.

Ruohoniemi, J. M., & Baker, K. B. (1998). Large-scale imaging of high-latitude convection with Super Dual Auroral Radar Network HF radar observations. *Journal of Geophysical Research*, *103*, 20,797–20,811. https://doi.org/10.1029/98JA01288

Ruohoniemi, J. M., & Greenwald, R. A. (2005). Dependencies of high-latitude plasma convection: Consideration of interplanetary magnetic field, seasonal, and universal time factors in statistical patterns. *Journal of Geophysical Research*, *110*, A09204. https://doi.org/10.1029/2004JA010815

Shepherd, S., & Ruohoniemi, J. (2000). Electrostatic potential patterns in the high-latitude ionosphere constrained by SuperDARN measurements. *Journal of Geophysical Research*, *105*, 23,005–23,014.

Smith, C. W., L'Heureux, J., Ness, N. F., Acuña, M. H., Burlaga, L. F., & Scheifele, J. (1998). The ACE magnetic fields experiment. *Space Science Reviews*, *86*, 613–632. https://doi.org/10.1023/A:1005092216668

Tenfjord, P., Ostgaard, N., Strangeway, R., Haaland, S., Snekvik, K., Laundal, K. M., … Milan, S. E. (2017). Magnetospheric response and reconfiguration times following IMF B_y reversals. *Journal of Geophysical Research: Space Physics*, *122*, 417–431. https://doi.org/10.1002/2016JA023018

Watanabe, M., Sofko, G. J., Kabin, K., Rankin, R., Ridley, A. J., Clauer, C. R., & Gombosi, T. I. (2007). Origin of the interhemispheric potential mismatch of merging cells for interplanetary magnetic field B_y-dominated periods. *Journal of Geophysical Research*, *112*, A10205. https://doi.org/10.1029/2006JA012179

Weimer, D. R. (1999). Substorm influence on the ionospheric electric potentials and currents. *Journal of Geophysical Research*, *104*, 185–198. https://doi.org/10.1029/1998JA900075

Weimer, D. R. (2001). An improved model of ionospheric electric potentials including substorm perturbations and application to the geospace environment modeling November 24, 1996, event. *Journal of Geophysical Research*, *106*(A1), 407–416. https://doi.org/10.1029/2000JA000604

Weimer, D. R. (2005). Improved ionospheric electrodynamic models and application to calculating joule heating rates. *Journal of Geophysical Research*, *110*, A05306. https://doi.org/10.1029/2004JA010884

Zou, S., Lyons, L. R., Wang, C. P., Boudouridis, A., Ruohoniemi, J. M., Anderson, P. C., … Devlin, J. C. (2009). On the coupling between the harang reversal evolution and substorm dynamics: A synthesis of SuperDARN, DMSP, and IMAGE observations. *Journal of Geophysical Research*, *114*, A01205. https://doi.org/10.1029/2008JA013449

Zou, S., Moldwin, M. B., Lyons, L. R., Nishimura, Y., Hirahara, M., Sakanoi, T., … Heinselman, C. J. (2010). Identification of substorm onset location and preonset sequence using Reimei, THEMIS GBO, PFISR, and Geotail. *Journal of Geophysical Research*, *115*, A12309. https://doi.org/10.1029/2010JA015520